Research Square

Preprints are preliminary reports that have not undergone peer review.
They should not be considered conclusive, used to inform clinical practice,
or referenced by the media as validated information.

Network-structured Ru/RuO 2 -FeNiCo-LDH as a high-performance bifunctional electrocatalyst for overall water splitting

Aoxing Zhao
Hefei Normal University
Sibei Li
Hefei Normal University
Shun Wang
Southeast University
Zhe Jia
Southeast University
Zhengxi Guo
Hefei Normal University
Miao Zhang
Anhui University
Lei Yang
Hefei University
Jianguo Lv
jglv@hfnu.edu.cn

Hefei Normal University

Research Article

Keywords: HER, OER, FeNiCo-LDH, OWS, Ru/RuO2

Posted Date: November 2nd, 2026

DOI: https://doi.org/10.21203/rs.3.rs-11326799/v1

License: This work is licensed under a Creative Commons Attribution 4.0 International License.
Read Full License

Additional Declarations: No competing interests reported.

Abstract

Rationally designing and synthesizing efficient bifunctional electrocatalysts is crucial for overall water splitting (OWS). Herein, a Ru/RuO_2-FeNiCo-LDH/NF electrocatalyst with an interconnected porous network was fabricated on nickel foam (NF) via electrodeposition followed by precursor combustion. At a current density of 10 mA cm^{-2}, Ru/RuO_2-Fe-0.1-Co-0.1-LDH/NF requires overpotentials of 52 mV and 205 mV in 1 M KOH for the hydrogen evolution reaction (HER) and oxygen evolution reaction (OER), respectively. A two-electrode electrolyzer using Ru/RuO_2-Fe-0.1-Co-0.1-LDH/NF as both electrodes requires a cell voltage of 1.40 V to reach a current density of 10 mA cm^{-2}. The interconnected porous network, Ru/RuO_2 active species, low charge-transfer resistance (R_{ct} = 13.7 Ω), and large electrochemically active surface area (ECSA = 704.5 cm^2) synergistically contribute to efficient OWS. This work offers new insights into developing efficient bifunctional electrocatalysts for OWS.

1. Introduction

The combustion of fossil fuels has given rise to growing environmental crises, and the exploration of clean energy underpins the sustainable development of humanity [1–3]. As a green energy carrier, hydrogen offers advantages including high energy density, abundant reserves, and zero environmental pollution, making it promising for the clean energy transition [4, 5]. Water electrolysis driven by renewable electricity represents an efficient and eco-friendly strategy for hydrogen generation. Currently, mainstream commercial electrocatalysts are noble-metal-based, and different catalysts are typically used for the hydrogen evolution reaction (HER) and oxygen evolution reaction (OER), such as Pt for HER [6] and RuO_2 and IrO_2 for OER [7–9]. The limited availability and high cost of noble metals hinder their large-scale industrial application. HER and OER electrocatalysts differ in optimal reaction conditions and may induce cross-contamination, increasing the complexity and operational costs of overall water splitting (OWS) [10]. Therefore, it is important to develop low-cost electrocatalysts with high HER and OER activities under the same reaction conditions.

Transition-metal layered double hydroxides (TM-LDHs) are considered promising OER electrocatalysts due to their abundant intrinsic active sites and high specific surface areas, which promote effective charge and mass transfer during the oxygen evolution process [11–14]. Su et al. [14] prepared 3D flower-like Fe-doped NiCo-LDH (NCF-LDH) via a hydrothermal process followed by etching with a ferric chloride hexahydrate solution. In alkaline media, the NCF-LDH electrode exhibits an overpotential of 263 mV at 50 mA cm^{-2}, a low Tafel slope of 71.9 mV dec^{-1}, and good operational stability. Liu et al. [13] fabricated a high-efficiency NiFe-LDH@CS heterostructure via two-step hydrothermal synthesis. Under optimized preparation conditions, the NiFe-LDH@CS heterostructure exhibits high OER activity, with overpotentials of 292 mV at 50 mA cm^{-2} and 372 mV at 100 mA cm^{-2}. Accordingly, improving the HER performance of TM-LDH catalysts with high OER activity is important for achieving bifunctional electrocatalysis [15, 16]. Multiple modification strategies including heteroatom doping, interface modulation and electronic structure regulation have been developed to boost electrical conductivity, expose abundant active sites

and accelerate water dissociation kinetics for high-efficiency OWS [17–20]. Baig et al. [21] prepared NiMn-LDH via a sonochemical route. The NiMn-LDH-4h electrode delivers a current density of 10 mA cm^{-2} at overpotentials of 120 mV and 296 mV in 1 M KOH for HER and OER, respectively. Furthermore, the symmetric electrolyzer assembled with NiMn-LDH-4h as both the cathode and anode achieves a current density of 10 mA cm^{-2} at 1.6 V for OWS. Yao et al. [22] coupled NiTe nanorods onto amorphous CoFe-LDH by electrodeposition, constructing hierarchical NiTe@CoFe-LDH heterostructures. The NiTe@CoFe-LDH electrocatalyst requires low overpotentials of 218 mV and 103 mV to reach 10 mA cm^{-2} for the OER and HER, respectively, and maintains stable performance for 50 h. The symmetric NiTe@CoFe-LDH electrolyzer requires only 1.56 V to reach a current density of 10 mA cm^{-2}. These results highlight the potential of this electrode for green hydrogen production. Gao et al. [23] engineered NiFe-BLDH@Ru-$Ni(OH)_2$/NF via a simple two-step synthetic strategy. The distinctive 2D/2D hierarchical heterostructure expedites interfacial charge migration and enriches accessible electroactive sites. The embedded Ru nanoparticles serve as dual-active centers to accelerate both HER and OER kinetics, resulting in outstanding bifunctional electrocatalytic performance. In 1.0 M KOH electrolyte, NiFe-BLDH@Ru-$Ni(OH)_2$/NF requires overpotentials of 249 mV for OER and 138 mV for HER at 100 mA cm^{-2}. Given the outstanding intrinsic HER activity of noble metals (Pt, Ir, Ru, etc.) and their oxides, decorating transition metal-based LDHs with trace amounts of noble metals can drastically boost HER activity and thus endow the electrocatalysts with overall water-splitting performance[24, 25]. However, FeNiCo-LDH catalysts incorporating low loadings of Ru/RuO_2 for efficient OWS remain largely unexplored.

Herein, we fabricated a novel Ru/RuO_2-FeNiCo-LDH/NF electrocatalyst featuring an interconnected porous network structure via electrodeposition followed by precursor combustion. Owing to the synergistic effects between the Ru/RuO_2 and FeNiCo-LDH components, the resulting catalyst exhibits low overpotentials of 205 m*V* and 52 m*V* for OER and HER, respectively. Benefiting from its excellent bifunctional activity, the symmetric electrolyzer assembled with Ru/RuO_2-Fe-0.1-Co-0.1-LDH/NF enables OWS at a low operating voltage of 1.40 *V* at 10 mA cm^{-2} and maintains stable operation for 100 h.

2. Experimental

2.1. Preparation of NiCo-LDH/NF and FeNiCo-LDH/NF

NiCo-LDH/NF and FeNiCo-LDH/NF were prepared by cathodic electrodeposition on nickel foam (NF) using a three-electrode system in chronoamperometric (*i-t*) mode. Cobalt nitrate was dissolved in 50 mL of deionized water, and the solution was magnetically stirred for 30 min to obtain a homogeneous solution. The deposition potential was set at -2.5 V vs. Ag/AgCl, and the deposition time was 600 s. Samples synthesized with 0.05, 0.10, and 0.25 mol L^{-1} cobalt nitrate in the electrolyte were denoted as Co-0.05-LDH/NF, Co-0.1-LDH/NF and Co-0.25-LDH/NF, respectively. Fe-0.1-Co-0.1-LDH/NF was electrodeposited in an aqueous electrolyte containing equimolar cobalt nitrate and ferric nitrate. After

electrodeposition, the samples were rinsed repeatedly with ethanol and deionized water to remove surface residues and then dried in air at 60°C.

2.2. Preparation of Ru/RuO_2-Fe-0.1-Co-0.1-LDH/NF

Ru/RuO_2-Fe-0.1-Co-0.1-LDH/NF was synthesized via a one-step precursor combustion strategy, following the procedure reported in the literature [26]. Briefly, a 0.05 mol L^{-1} solution of ruthenium trichloride in ethanol was prepared. Then, the obtained Fe-0.1-Co-0.1-LDH/NF was immersed in the resulting solution for 1 min. The Fe-0.1-Co-0.1-LDH/NF precursor was removed from the solution and ignited in ambient air until the flame extinguished, yielding the final Ru/RuO_2-Fe-0.1-Co-0.1-LDH/NF product. The synthetic procedure of Ru/RuO_2-Fe-0.1-Co-0.1-LDH/NF is illustrated in Fig. 1.

2.3. Characterization and Electrochemical Measurements

The detailed procedures are provided in the Supplementary Information.

3. Results and discussion

3.1. Structural characterization

X-ray diffraction (XRD) patterns of Co-0.05-LDH/NF, Co-0.1-LDH/NF, Co-0.25-LDH/NF, Fe-0.1-Co-0.1-LDH/NF and Ru/RuO_2-Fe-0.1-Co-0.1-LDH/NF are shown in Fig. S1 and Fig. 2a. Three prominent diffraction peaks at 2θ = 44.5°, 51.8° and 76.4° in all samples are assigned to the (111), (200) and (220) planes of cubic Ni, respectively (PDF 04-0850). For Co-0.05-LDH/NF, Co-0.1-LDH/NF and Co-0.25-LDH/NF, two weak diffraction peaks at approximately 2θ = 19.5° and 38.6° are assigned to the (006) and (015) planes of NiCo-LDH, respectively. In addition to these two diffraction peaks, Fe-0.1-Co-0.1-LDH/NF exhibits a peak at 2θ = 33.3° that can be indexed to the (202) plane of $Fe(OH)_3$ (PDF 46-1436). For Ru/RuO_2-Fe-0.1-Co-0.1-LDH/NF, three diffraction peaks at 2θ = 37.2°, 43.7° and 62.8° can be indexed to the (111), (200) and (220) planes of cubic NiO, respectively (PDF 47-1049). Two diffraction peaks at 2θ = 35.1 ° and 57.9 ° can be indexed to the (101) and (220) crystal planes of RuO_2 (PDF 43-1027). The scanning electron microscopy (SEM) image of Ru/RuO_2-Fe-0.1-Co-0.1-LDH/NF (Fig. 2b) shows randomly distributed two-dimensional thin nanosheets that interconnect to form a porous network. This network can facilitate electrolyte penetration and mass transfer and improve active-site accessibility, thereby contributing to the electrocatalytic performance. Transmission electron microscopy (TEM) observations further corroborate the formation of the interconnected porous network, as shown in Fig. 2c. As shown in the high-resolution TEM (HRTEM) images (Fig. 2d, e), the measured interplanar spacings of 0.225 nm and 0.205 nm correspond to the (200) plane of rutile RuO_2 and the (101) plane of Ru, respectively. The interplanar spacings of 0.153 nm and 0.241 nm correspond to the (110) plane of NiCo-LDH and the (111) plane of NiO, respectively. As shown in Fig. 2f, elemental mapping confirms the coexistence of Fe, Co, Ni, Ru and O, which are uniformly distributed throughout Ru/RuO_2-Fe-0.1-Co-0.1-LDH/NF.

To examine the surface composition and elemental oxidation states, X-ray photoelectron spectroscopy (XPS) was performed on Fe-0.1-Co-0.1-LDH/NF and Ru/RuO_2-Fe-0.1-Co-0.1-LDH/NF. The XPS survey spectrum of Ru/RuO_2-Fe-0.1-Co-0.1-LDH/NF confirms the coexistence of Fe, Co, Ni and Ru (Fig. 3a). In the Fe 2p spectra presented in Fig. 3b, the peaks at approximately 710.5 eV and 723.5 eV are assigned to the Fe $2p_{3/2}$ and Fe $2p_{1/2}$ components of Fe^{2+}, respectively, whereas those near 711.9 eV ($2p_{3/2}$) and 725.3 eV ($2p_{1/2}$) originate from Fe^{3+}. The shake-up satellite peaks located at 718.8 eV and 732.0 eV further confirm the presence of Fe species [27, 28]. The Co 2p spectra (Fig. 3c) can be deconvoluted into six distinct peaks. The characteristic peaks at 779.8 and 795.4 eV correspond to the Co $2p_{3/2}$ and Co $2p_{1/2}$ components of Co^{3+}, respectively. The other two peaks at 781.1 and 797.1 eV are assigned to the Co $2p_{3/2}$ and Co $2p_{1/2}$ components of Co^{2+}, [29, 30]. In addition, two satellite peaks are observed at binding energies of 785.1 and 802.9 eV [31]. The Ni 2p spectra (Fig. 3d) exhibit two distinct peaks at 855.1 eV and 872.9 eV, which are assigned to the Ni $2p_{3/2}$ and Ni $2p_{1/2}$ components of Ni^{3+}, [29, 32]. The signals at 856.6 eV and 874.4 eV are assigned to the Ni $2p_{3/2}$ and Ni $2p_{1/2}$ components of Ni^{2+}, [33, 34], while satellite peaks appear at 861.5 and 879.6 eV. The high-resolution O 1s spectra (Fig. 3e) can be deconvoluted into three components at 529.6, 531.1, and 532.8 eV, assigned to metal-oxygen (M-O) species, hydroxyl species (-OH), and adsorbed molecular water, respectively[27, 35]. Compared with Fe-0.1-Co-0.1-LDH/NF, Ru/RuO_2-Fe-0.1-Co-0.1-LDH/NF exhibits a higher relative content of M-O species associated with nickel and ruthenium oxides [31, 36]. This finding is consistent with the XRD characterization results. The high-resolution Ru 3d spectrum of Ru/RuO_2-Fe-0.1-Co-0.1-LDH/NF partially overlaps with the C 1s spectrum (Fig. 3f). The two characteristic peaks at 280.5 and 284.4 eV correspond to the Ru $3d_{5/2}$ and Ru $3d_{3/2}$ components of Ru^0, [37], and the peaks at 281.9 eV and 285.7 eV correspond to the Ru $3d_{5/2}$ and Ru $3d_{3/2}$ components of Ru^{4+}, [31]. Three additional peaks at 288.9, 286.5, and 284.8 eV are assigned to the C = O, C-O, and C-C groups, respectively[31, 38].

3.2. Electrocatalytic performance

The electrocatalytic performance of Co-0.05-LDH/NF, Co-0.1-LDH/NF, Co-0.25-LDH/NF, Fe-0.1-Co-0.1-LDH/NF and Ru/RuO_2-Fe-0.1-Co-0.1-LDH/NF was assessed in 1.0 M KOH electrolyte using a standard three-electrode setup. The HER linear sweep voltammetry (LSV) curves are shown in Fig. 4a, and the corresponding overpotentials for each electrode are summarized in Fig. 4b. Ru/RuO_2-Fe-0.1-Co-0.1-LDH/NF requires an overpotential of only 52 mV at 10 mA cm^{-2}, lower than those of Co-0.05-LDH/NF (η_{10} = 184 mV), Co-0.1-LDH/NF (η_{10} = 156 mV), Co-0.25-LDH/NF (η_{10} = 171 mV), and Fe-0.1-Co-0.1-LDH/NF (η_{10} = 96 mV). This result demonstrates its outstanding HER electrocatalytic activity. Figure 4c shows the Tafel plots of all electrocatalysts. Ru/RuO_2-Fe-0.1-Co-0.1-LDH/NF exhibits the lowest Tafel slope, 66.4 mV dec^{-1}, indicating favorable HER kinetics. The OER polarization curves of these as-prepared electrodes are presented in Fig. 4d. Figure 4e shows that Ru/RuO_2-Fe-0.1-Co-0.1-LDH/NF requires the lowest OER overpotential, 205 mV at 10 mA cm^{-2}, compared with Co-0.05-LDH/NF (η_{10} =

314 mV), Co-0.1-LDH/NF (η_{10} = 255 mV), Co-0.25-LDH/NF (η_{10} = 293 mV), and Fe-0.1-Co-0.1-LDH/NF (η_{10} = 221 mV). The Tafel slope of Ru/RuO_2-Fe-0.1-Co-0.1-LDH/NF is 31.9 mV dec^{-1}, lower than those of Co-0.05-LDH/NF (53.4 mV dec^{-1}), Co-0.1-LDH/NF (45.2 mV dec^{-1}), Co-0.25-LDH/NF (76.5 mV dec^{-1}), and Fe-0.1-Co-0.1-LDH/NF (33.1 mV dec^{-1}) (Fig. 4f), suggesting more favorable OER kinetics. Electrochemical impedance spectroscopy (EIS) measurements were performed to investigate charge-transfer kinetics, and the results are shown in Fig. 4g. Following Ru/RuO_2 deposition, the Nyquist plot of the Ru/RuO_2-Fe-0.1-Co-0.1-LDH/NF electrode exhibits a smaller semicircle than those of the other electrodes. The Nyquist plots were fitted using an equivalent circuit model to obtain the charge-transfer resistance (R_{ct}) of each electrode (Table S1). Among the tested electrodes, Ru/RuO_2-Fe-0.1-Co-0.1-LDH/NF exhibits the lowest R_{ct}, 13.7 Ω. The ECSA of an electrocatalyst is directly proportional to its double-layer capacitance (C_{dl}) (Fig. 4h, Table S2). C_{dl} was obtained from cyclic voltammetry (CV) curves measured in the non-Faradaic region (Fig. S5-S9). The ECSA values of the electrocatalysts are listed in Table S2. Ru/RuO_2-Fe-0.1-Co-0.1-LDH/NF exhibits the highest C_{dl} among the tested electrodes, 28.18 mF cm^{-2}. This result indicates that Ru/RuO_2-Fe-0.1-Co-0.1-LDH/NF has the largest estimated ECSA among the tested electrodes. This large ECSA may be associated with the Ru/RuO_2 modification and the interconnected porous network, which facilitate active-site accessibility. Long-term chronoamperometric measurements at 10 mA cm^{-2} demonstrate that the Ru/RuO_2-Fe-0.1-Co-0.1-LDH/NF electrode maintains stable HER and OER performance during continuous operation for 48 h (Fig. 4i).

Given the high bifunctional activity of Ru/RuO_2-Fe-0.1-Co-0.1-LDH/NF for HER and OER in 1.0 M KOH electrolyte, an electrolyzer for OWS was assembled using this electrocatalyst as both the anode and cathode. LSV curves of the electrolyzers assembled with Ru/RuO_2-Fe-0.1-Co-0.1-LDH/NF and the commercial Pt/C//IrO_2:RuO_2 couple are shown in Fig. 5a. For OWS, the electrolyzer assembled with Ru/RuO_2-Fe-0.1-Co-0.1-LDH/NF achieves a current density of 10 mA cm^{-2} at a cell voltage of 1.40 *V*, lower than the 1.54 *V* required by Pt/C//IrO_2:RuO_2. Comparisons with recently reported bifunctional electrocatalysts are presented in Fig. 5b and Table S3. The electrolyzer also exhibits stable performance during a 100 h chronoamperometric test (Fig. 5c). In addition, the electrolyzer can also be driven by a solar panel with an output voltage of approximately 1.54 *V* (Video S1). Steady bubble evolution can be clearly observed on the surfaces of both electrodes. These results suggest the potential of Ru/RuO_2-Fe-0.1-Co-0.1-LDH/NF for solar-powered hydrogen production.

4. Conclusions

In summary, Ru/RuO_2-Fe-0.1-Co-0.1-LDH/NF was successfully fabricated via electrodeposition followed by precursor combustion. The electrocatalyst exhibits an interconnected porous network formed by interwoven two-dimensional ultrathin nanosheets. This structure can facilitate electrolyte penetration and mass transfer and improve the accessibility of HER and OER active sites, thereby contributing to the electrocatalytic performance. To reach a current density of 10 mA cm^{-2}, Ru/RuO_2-Fe-0.1-Co-0.1-LDH/NF

requires overpotentials of 52 m*V* and 205 m*V* for HER and OER, respectively. The electrolyzer assembled with Ru/RuO_2-Fe-0.1-Co-0.1-LDH/NF for OWS requires a cell voltage of only 1.40 *V* to achieve a current density of 10 mA cm^{-2}. The enhanced OWS performance may be attributed to the low charge-transfer resistance (R_{ct} = 13.7 Ω), large ECSA (704.5 cm^2), interconnected porous network, and Ru/RuO_2 active species. This work provides insights into the design and fabrication of advanced electrocatalysts for energy conversion and storage.

Declarations

Declaration of AI use

The authors declare that the manuscript was entirely human-written. AI-assisted tools (Doubao) were only employed for language proofreading, grammar correction and wording refinement.

Author Contribution

A. Zhao, S. Li and J. Lv wrote the main manuscript. A. Zhao, Z. Guo, M. Zhang, M. Zhao and L. Yang synthesized the electrocatalysts and performed the electrochemical measurements and overall water splitting tests. S. Wang and Z. Jia contributed to data analysis and interpretation. All authors reviewed the manuscript.

Acknowledgements

This work was supported by the Natural Science Foundation of Anhui Higher Education Institution of China (No. 2023AH040160) and the Graduate Innovation Fund Project of Hefei Normal University in 2026 (2026yjs051).

References

1. Zhou G, Xu L, Hu G, Mai L, Cui Y (2019) Nanowires Electrochem Energy Storage Chem Reviews 119:11042–11109
2. Xue Z-H, Luan D, Zhang H, Lou XW (2022) Single-atom catalysts for photocatalytic energy conversion. Joule 6:92–133
3. Tiwari JN, Sultan S, Myung CW, Yoon T, Li N, Ha M, Harzandi AM, Park HJ, Kim DY, Chandrasekaran SS, Lee WG, Vij V, Kang H, Shin TJ, Shin HS, Lee G, Lee Z, Kim KS (2018) Multicomponent electrocatalyst with ultralow Pt loading and high hydrogen evolution activity. Nat Energy 3:773–782
4. Yang J, Mohmad AR, Wang Y, Fullon R, Song X, Zhao F, Bozkurt I, Augustin M, Santos EJG, Shin HS, Zhang W, Voiry D, Jeong HY, Chhowalla M (2019) Ultrahigh-current-density niobium disulfide catalysts for hydrogen evolution. Nat Mater 18:1309–1314

5. Ring L, Pollet BG, Chatenet M, Abbou S, Küpper K, Schmidt M, Huck M, Gries A, Steinhart M, Schäfer H (2019) From Bad Electrochemical Practices to an Environmental and Waste Reducing Approach for the Generation of Active Hydrogen Evolving Electrodes. Angew Chem Int Ed 58:17383–17392
6. Luo W, Gan J, Huang ZK, Chen WY, Qian G, Zhou XG, Duan XZ (2019) Boosting HER Performance of Pt-Based Catalysts Immobilized on Functionalized Vulcan Carbon by Atomic Layer Deposition. Front Mater, 6
7. Yang J, Shen Y, Sun Y, Xian J, Long Y, Li G (2023) Ir Nanoparticles Anchored on Metal-Organic Frameworks for Efficient Overall Water Splitting under pH-Universal Conditions. Angew Chem 135:e202302220
8. Beppu K, Obigane K, Amano F (2023) Amorphous versus nanocrystalline RuO_2 electrocatalysts: activity and stability for oxygen evolution reaction in sulfuric acid Electronic supplementary information (ESI) available, vol 13. Catalysis Science & Technology, pp 6653–6661
9. Tang L, Chen X, Xie Z, Xiang Q, Liu J, Li L, Wei Z (2025) Metal–oxygen bonding characteristics dictate activity and stability differences of RuO2 and IrO2 in the acidic oxygen evolution reaction. Phys Chem Chem Phys 27:9369–9378
10. Kim M, Kim Y, Ha MY, Shin E, Kwak SJ, Park M, Kim I, Jung WB, Lee WB, Kim Y, Jung HT (2023) Exploring Optimal Water Splitting Bifunctional Alloy Catalyst by Pareto Active Learning. Adv Mater, 35
11. Chen S, Yu C, Cao ZF, Huang XP, Wang S, Zhong H (2021) Trimetallic NiFeCr-LDH/MoS2 composites as novel electrocatalyst for OER. Int J Hydrog Energy 46:7037–7046
12. Li LT, Xiao LF, Cheng X, Li SD, Tian T, Wang YD, Tang HL (2025) NiFe-LDH modified cobalt boride for enhanced OER catalytic performance. Electrochim Acta, 539
13. Liu DX, Yang Y, Zhang JA, Wang LM, Ma ZW, Ren L, Wang JQ, Xue B, Li FF (2023) Improved OER catalytic performance of NiFe-LDH with hydrothermal carbonization microspheres. J Alloys Compd, 941
14. Su WX, Jia JJ, Zhou Q, Feng CC (2026) Fe-doped 3D flower-like NiCo-LDH for enhanced OER performance. Ionics 32:4393–4405
15. Mondal PVP, Mukherjee D, Laha S, Sarkar S (2026) Optimizing Ni/Co ratios in NiCo-LDH for enhanced hydrogen and oxygen evolution reactions in overall water splitting. J Power Sources 671:239607
16. Guo X, Cai B, Tao K (2026) Heterostructured Co2P@NiFe LDH as an efficient bifunctional electrocatalyst for overall water splitting. Int J Hydrog Energy 233:155045
17. Zhang J, Liu J, Xi L, Yu Y, Chen N, Sun S, Wang W, Lange KM, Zhang B (2018) Single-Atom Au/NiFe Layered Double Hydroxide Electrocatalyst: Probing the Origin of Activity for Oxygen Evolution Reaction. J Am Chem Soc 140:3876–3879
18. Liu L, Liu H, Jia B, Qu X, Qin M (2025) Durable Pt-Decorated NiFe-LDH for High-Current-Density Electrocatalytic Water Splitting Under Alkaline Conditions, Nanomaterials, 15 1683

19. Tian Y, Li J, Li F, Wang R, Liu J, Ma J (2025) Ru/Ni3S2/NiFe LDH with Multiple Heterogeneous Interfaces as Active Electrocatalyst for Boosted Hydrogen Evolution Reaction. Ind Eng Chem Res 64:15165–15170
20. Yao H, Wang S, Cao Y, Chen R, Lu Z, Hu J, Xie J, Hao A (2022) High-performance bifunctional electrocatalysts of CoFe-LDH/NiCo2O4 heterostructure supported on nickel foam for effective overall water splitting. J Alloys Compd 926:166846
21. Baig MM, Gul IH, Ahmad R, Baig SM, Khan MZ, Iqbal N (2021) One-step sonochemical synthesis of NiMn-LDH for supercapacitors and overall water splitting. J Mater Sci 56:18636–18649
22. Yao L, Li R, Zhang H, Humayun M, Xu X, Fu Y, Nikiforov A, Wang C (2022) Interface engineering of NiTe@CoFe LDH for highly efficient overall water-splitting. Int J Hydrog Energy 47:32394–32404
23. Gao H-H, Gao T, Wang W, Xie K-F, Zhao X, Liu Z-H (2026) Synergistic borate anion-intercalated and Ru decoration in 2D/2D NiFe-LDH@Ni(OH)2 heterostructure for boosting overall water splitting. J Alloys Compd 1050:185645
24. Yu G, Shi R, Chen C, Wu D, Zhou C, Wang P (2025) Ultrafine and low-loading Pt nanoparticles anchored in NiFe-LDH as overall water splitting electrocatalyst. Int J Hydrog Energy 166:150892
25. Tan L, Wang H, Qi C, Peng X, Pan X, Wu X, Wang Z, Ye L, Xiao Q, Luo W, Gao H, Hou W, Li X, Zhan T (2024) Regulating Pt electronic properties on NiFe layered double hydroxide interface for highly efficient alkaline water splitting. Appl Catal B 342:123352
26. Niu X-J, Ma Y-L, Gao J-Y, Lu Z-H, Li J-S (2025) Interfacial engineering of RuO2/CoOOH heterojunction for efficient oxygen evolution reaction. J Alloys Compd 1025:180409
27. Wu S-W, Liu S-Q, Tan X-H, Zhang W-Y, Cadien K, Li Z (2022) Ni3S2-embedded NiFe LDH porous nanosheets with abundant heterointerfaces for high-current water electrolysis. Chem Eng J 442:136105
28. Huang J, Han J, Wang R, Zhang Y, Wang X, Zhang X, Zhang Z, Zhang Y, Song B, Jin S (2018) Improving Electrocatalysts for Oxygen Evolution Using NixFe3–xO4/Ni Hybrid Nanostructures Formed by Solvothermal Synthesis. ACS Energy Lett 3:1698–1707
29. Bai L, Cao W, Du X, Wang Y, Wu L, Li J (2023) Cobalt and vanadium dual-doping engineering of NiS/Ni7S6 with heterogeneous interface as efficient electrocatalyst for the oxygen evolution reaction. J Alloys Compd 960:170652
30. Duan J-J, Zhang R-L, Feng J-J, Zhang L, Zhang Q-L, Wang A-J (2021) Facile synthesis of nanoflower-like phosphorus-doped Ni3S2/CoFe2O4 arrays on nickel foam as a superior electrocatalyst for efficient oxygen evolution reaction. J Colloid Interface Sci 581:774–782
31. Huang G, Wang C, Bukhvalov D, Yang Y, Gao J, Han F, Yang X, Wang C (2025) Hetero-interface triggering dynamic Ni(3+) active species in reduced Ru-doped NiCo-MOF to boost urea-assisted overall water splitting. Int J Hydrog Energy 145:84–94
32. Hung T-F, Yin Z-W, Betzler SB, Zheng W, Yang J, Zheng H (2019) Nickel sulfide nanostructures prepared by laser irradiation for efficient electrocatalytic hydrogen evolution reaction and supercapacitors. Chem Eng J 367:115–122

33. Zhai W, Chen Y, Liu Y, Ma Y, Vijayakumar P, Qin Y, Qu Y, Dai Z (2024) Covalently Bonded Ni Sites in Black Phosphorene with Electron Redistribution for Efficient Metal-Lightweighted Water Electrolysis. Nano-Micro Lett 16:115
34. Wang Y, Li X, Huang Z, Wang H, Chen Z, Zhang J, Zheng X, Deng Y, Hu W (2023) Amorphous Mo-doped NiS0.5Se0.5 Nanosheets@Crystalline NiS0.5Se0.5 Nanorods for High Current-density Electrocatalytic Water Splitting in Neutral Media. Angew Chem Int Ed 62:e202215256
35. Tran TTN, Hai ND, Ngo HD, Le TBN, Tran NQ (2025) Highly Electron-Deficient Ternary Metal Fluoride Nanocages for Overall Urea-Assisted Water Electrolysis. ACS Appl Energy Mater 8:3132–3144
36. Mu X, Yuan H, Jing H, Xia F, Wu J, Gu X, Chen C, Bao J, Liu S, Mu S (2021) Superior electrochemical water oxidation in vacancy defect-rich 1.5 nm ultrathin trimetal-organic framework nanosheets. Appl Catal B 296:120095
37. Wang H, Li X, Ruan Q, Tang J (2020) Ru and RuOx decorated carbon nitride for efficient ammonia photosynthesis. Nanoscale 12:12329–12335
38. Zhu K, Lei Q, Hu R, Zuo L, Lv J, Yu H, Zhao M, Wang C, Zhang M, Yang L (2025) Electrodeposition of ultra-low amount of Ru on FeCo-MOF/NF to enhance hydrogen production and methanol electroreforming performance. J Phys Chem Solids 207:112957

Figures

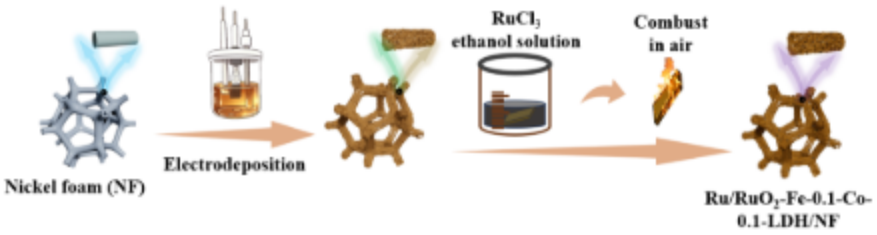


Figure 1

Synthetic procedure of Ru/RuO_2-Fe-0.1-Co-0.1-LDH/NF

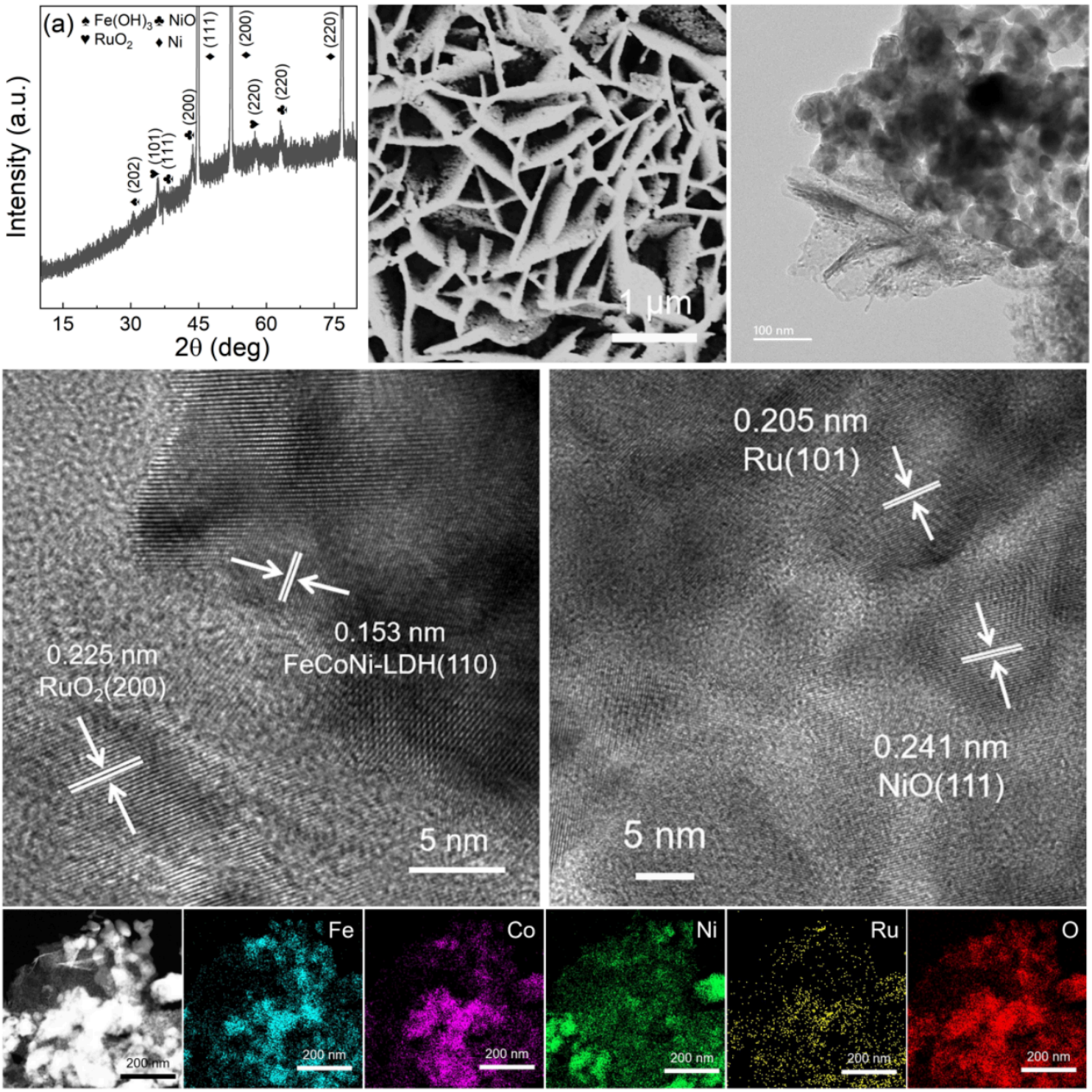


Figure 2

(a) XRD pattern, (b) SEM image, (c) TEM image, (d, e) HRTEM images, and (f) elemental mapping images of Ru/RuO_2-Fe-0.1-Co-0.1-LDH/NF

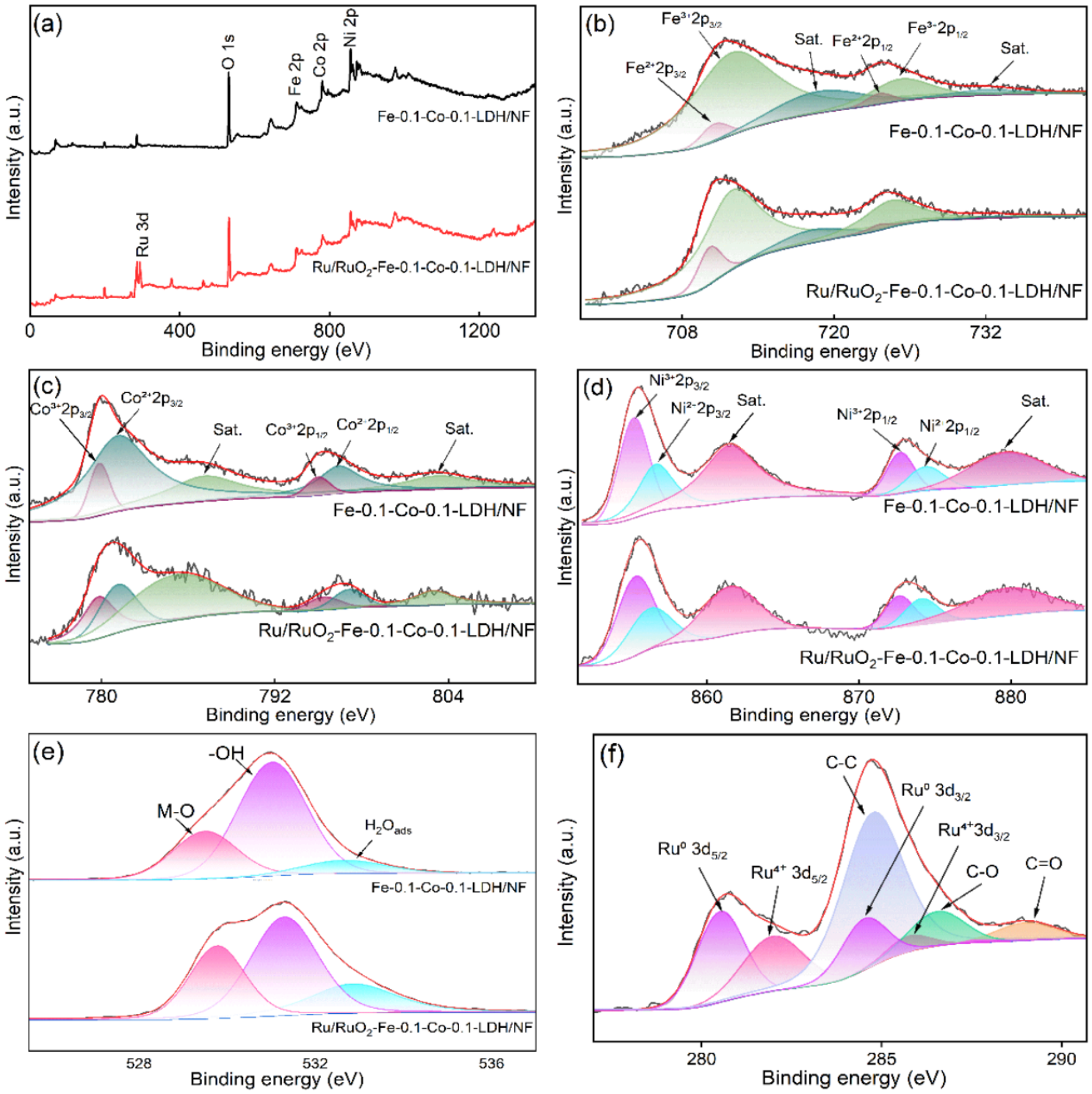


Figure 3

(a) XPS survey spectra and high-resolution spectra of (b) Fe 2p, (c) Co 2p, (d) Ni 2p, (e) O 1s, and (f) Ru 3d.

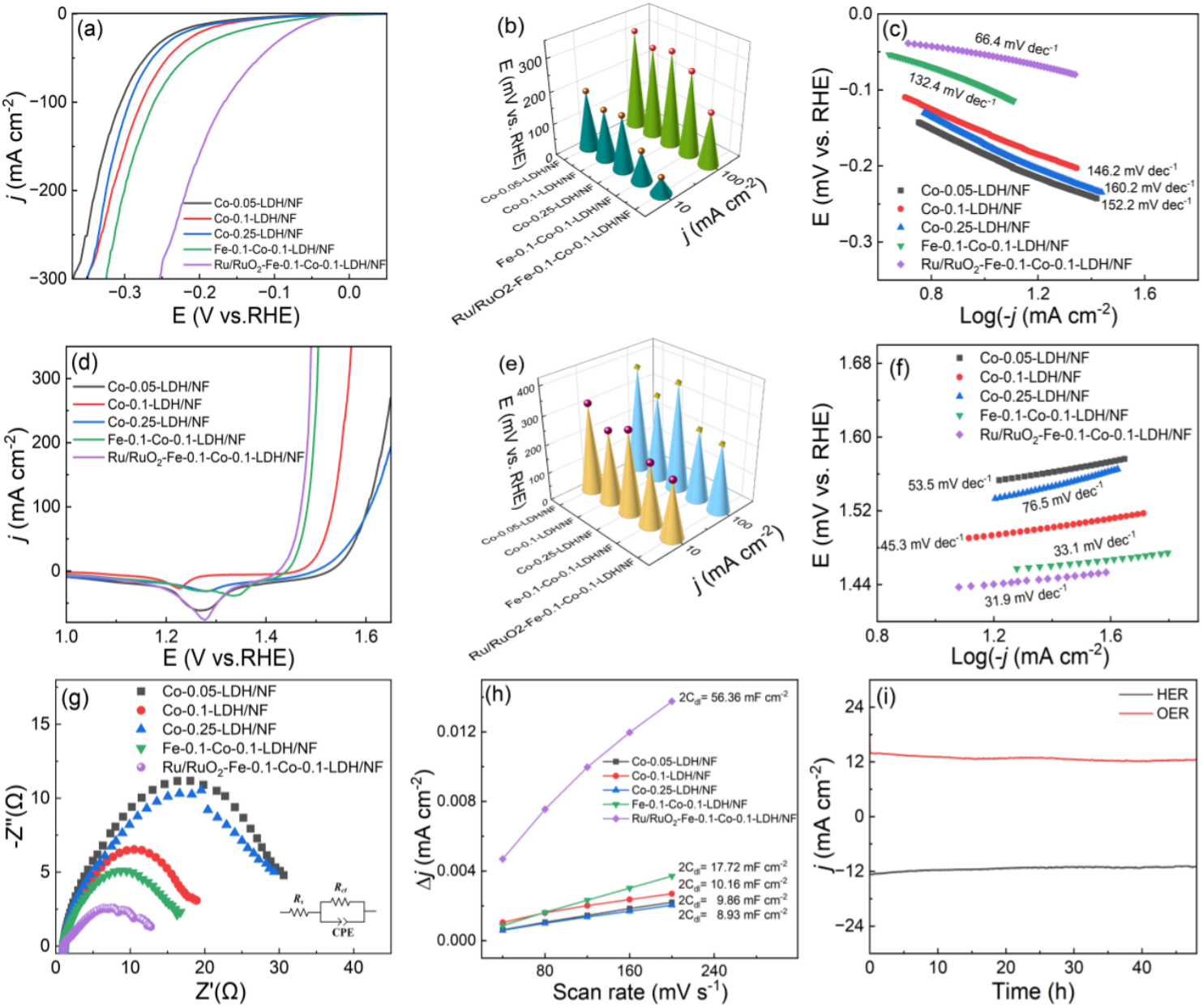


Figure 4

(a) LSV curves, (b) overpotentials at 10 and 100 mA cm^{-2}, and (c) Tafel plots for HER; (d) LSV curves, (e) overpotentials at 10 and 100 mA cm^{-2}, and (f) Tafel plots for OER; (g) Nyquist plots; and (h) double-layer capacitances (C_{dl}) of Co-0.05-LDH/NF, Co-0.1-LDH/NF, Co-0.25-LDH/NF, Fe-0.1-Co-0.1-LDH/NF and Ru/RuO_2-Fe-0.1-Co-0.1-LDH/NF. (i) Long-term chronoamperometric measurements of Ru/RuO_2-Fe-0.1-Co-0.1-LDH/NF for HER and OER over 48 h.

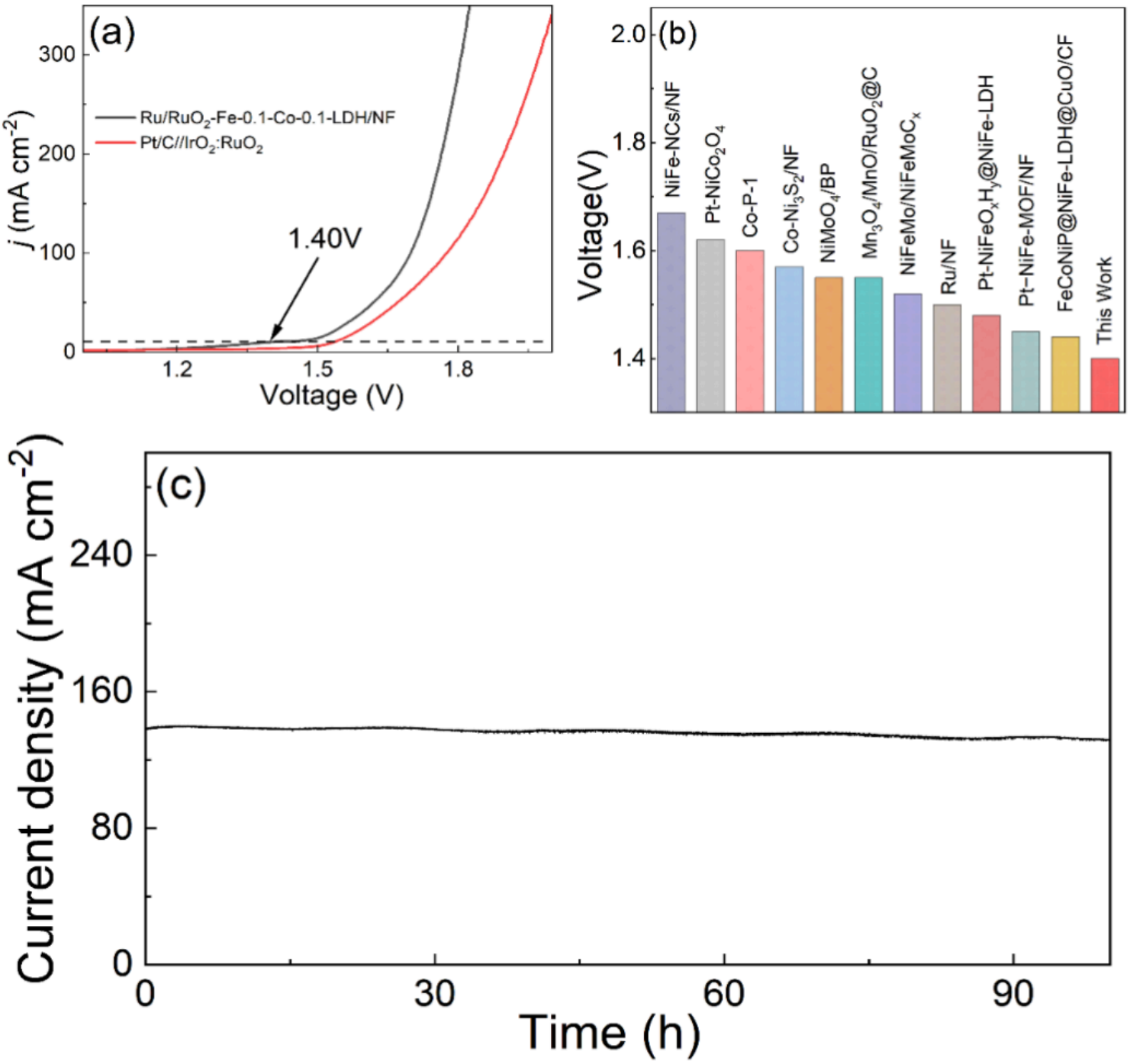


Figure 5

(a) LSV curves of the electrolyzer assembled with Ru/RuO_2-Fe-0.1-Co-0.1-LDH/NF for overall water splitting; (b) comparison of the cell voltages required by Ru/RuO_2-Fe-0.1-Co-0.1-LDH/NF and recently reported electrocatalysts; and (c) a long-term chronoamperometric test over 100 h.

Supplementary Files

This is a list of supplementary files associated with this preprint. Click to download.

- VideoS1.mp4
- SupplementaryInformation.docx